Supplementary Data:

Supplementary Materials and Methods:

Cell lines

L-Wnt3A cells (Cat: CRL2647^{TM}, ATCC, Manassas, VA), as well as HA-R-Spondin1-Fc293T (Trevigen, Gaithersburg, MD) cells were grown in DMEM medium supplemented with 10% fetal bovine serum (FBS) and antibiotics, and maintained in 37ºC humidified incubators, supplied with 5% CO2. Mycoplasma tests were performed weekly and only mycoplasma-free cells were utilized for experiments.

Conditioned medium

Conditioned media from L Wnt3A and HA-R-Spondin1-Fc293Twas obtained as previously described (32-36).

Immunohistochemistry and immunofluorescence

Fresh tissues as well as PDOs in culture were embedded into optimal cutting temperature compound (OCT) at -80 ºC. Tissue and PDO sections (8 uM) were prepared and stained. We utilized the following primary antibodies: LGR5 (stem cell marker Cat#: AP2745f, Abgent, San Diego, CA), SOX9 (stem cell marker- Cat#: 82630, Cell signaling, Danvers, MA), CK7 (biliary epithelium marker- Cat#: ab9021, Abcam, Cambridge, MA) and CK19 (biliary epithelium markers- Cat#: MAB3238 Millipore, Danvers, MA), EPCAM (epithelial marker- Cat#: 2929, Cell Signaling, Cell signaling, Danvers, MA), Hepatocyte Specific Antigen (Hep-Par1) (Cat#: 264R-1, Sigma Aldrich, St. Louis, MO). AFP (Cat# PA516658, ThermoFisher Scientific, Waltham, MA) Alexa Fluor dye-conjugated secondary antibodies (Life Technologies, Carlsbad, CA). Microphotographs were obtained with a Zeiss laser scanning microscope (LSM 510). Hematoxylin and Eosin (H&E) staining (Sigma Aldrich, St. Louis, MO), mucicarmine staining for mucin (Cat#: ab150667, Abcam, Cambridge, MA) were performed following standard protocols.Pictures were obtained with a Zeiss Axio Observer Inverted Microscope. For Live/Dead Cell image, Live cell marker Cell Tracker Green (Cat#: C7025, Life Technologies, Carlsbad, CA) and dead cell marker Ethidium homodimer

-1 (Cat#: E1169, Life Technologies, Carlsbad, CA) were utilized, Pictures were captured by Keyence BZ-X700 with Tokai Hit Incubator.

High-throughput RNA sequencing (RNA-Seq) and analysis

Total RNA was isolated from PDOs with passage 4 in culture using Trizol following the manufacturer's instructions. 100 nG of total RNA were utilized for RNA-Seq using HIseq4000 SE50 (BGI Hong Kong, China) with 50 or 75 bp paired-end reads. An average of 43 million reads were generated for each sample. The gene expression level was quantified using the RSEM software package by BGI (Hong Kong, China).

Supplementary Data:

Drug responses on PDO lines are reflective of tumor biology and not processing biases

To verify that the intra-patient and inter-patient drug response heterogeneity is indeed due to biology of the cancer and is not caused by the variability in establishment of PDO lines, we compared 2 sister PDO lines obtained from the same small piece of primary cancer. A 0.3 cm^3 piece of fresh human CCA tissue was split in 2 parts and each was utilized to establish a PDO line. Drug responses were recorded separately on these 2 sister PDO lines for each of the drugs in a 129-drug library. The paired sections showed similar responses to each of the 129 drugs, with ratios of cell viability ranging from 0.8-1.2. The results are shown in **Supplementary Table 13.**

Analysis of intra-tumor gene expression, somatic mutations and functional response

In order to explore the overall intra-tumor functional heterogeneity, we performed a PCA of the drug responses (**Supplementary Fig. 7a**, left-most panel). CCA8-7 and CCA8-11 had similar responses to drugs, as did CCA8-9, CCA8-10 and CCA8-5 amongst themselves, while CCA8-6 was dissimilar to the others (**Supplementary Fig. 7a**). Next, we built a PCA plot based on somatic mutations (**Supplementary Fig. 7a**, middle panel). We found low genetic divergence among four of the PDO lines (CCA8-5, CCA8-7, CCA8-9, and CCA8-11), with only 42 protein-coding single nucleotide variants exome-wide found to be polymorphic among these four lines, indicating a

likely common ancestor line. The other two PDO lines (CCA8-6 and CCA8-10) were genetically divergent in relation to each other, as well as to the group of the other four, indicating separate populations. We then built a phylogenetic tree based upon somatic mutations (**Supplementary Fig. 6**), which supports the PCA analysis and identified a subgroup of genetically similar PDOs (CCA8-5, 7, 9, and 11) and two others that were genetically divergent (CCA8-6 and CCA8-10). Next, we analyzed RNA data in a PCA analysis of the FPKM for each transcript in the NCBI human reference sequence database. We determined that the distribution of PDOs along the first and second principal components showed widely distributed heterogeneity, even among the four PDO lines that displayed genetic similarity in the exomic analysis above (**Supplementary Fig. 7a**, right-most panel). Using the first and second principal components of the DNA versus the RNA data, we found no statistically significant correlation for any drug, after Bonferroni correction for multiple testing for genes and drugs. In fact, the cluster of genetically similar PDOs (CCA8-5, CCA8-7, CCA8-9 and CCA8-11) described above did not cluster together in the PCA of transcripts, nor in the PCA for drug responses (**Fig. 7b**). Last, a univariate linear regression used to test for pairwise significant correlation (with Bonferroni correction for multiple testing) did not find any correlations between individual coding somatic DNA variants or expression levels of individual genes, and response profiles for each drug, across the 6 PDOs (**Fig. 7c.**).Taken together, the PCA did not suggest correlations between drug response and either gene expression or somatic mutations.

Supplementary Figure and Table Legends:

Supplementary Figure 1. Establishment of multi-region organoid lines from a primary human hepatocarcinoma. **(a)** The cancer resection piece was cut into 7 tissue slices as biologic replicates. The gross appearance of a miliary pattern of dissemination is consistent with a pathologic diagnosis of diffuse cirrhosis-like hepatocellular cancer. These tissues slices were utilized for histology, tissue banking, organoid establishment, and other analyses. **(b)** Bright field images of PDOs were recorded. Cystic patient derived organoid (PDO) structures started being

recognized at day 2 (D – day; P – passage). A cystic PDO was photographed from D1 to D13, at which point the culture was split. Images from P2, P5, and P10 are also shown, scale bar: 200 μm. **(c and d)** Immunofluorescence was performed on primary human cancer tissue and matched PDOs established from the same tissue slice for AFP and HepPar1 (hepatocyte markers), CK19 (cholangiocyte and hepatocyte marker), LGR5 (stem cell) and EPCAM (epithelial marker), scale bar: 100 μm. **(e and f)** Primary human cancer tissue and matched PDO established from the same tissue slice were used for hematoxylin and eosin staining, scale bar: 100 μm.

Supplementary Figure 2. Evaluation of cell death induced by gemcitabine. (a) 4X microscope magnification was utilized for these images. White light images demonstrate the typical cystic PDOs. Note that the NC – DMSO (negative control, DMSO – utilized to dilute drugs) did not induce any shrinking/collapse of the cystic PDO structures. PC – Triton X (positive control, Triton X 10% treated cells) demonstrated no intact PDO structures. Gemcitabine treated cells demonstrated smaller PDO structures, but it is not clear in the white light images if any cell death occurred or the effects were due to lack of growth. Therefore, we utilized the live cell marker Cell Tracker Green (green in the figure, Life Technologies, Carlsbad, CA) and dead cell marker Ethidium homodimer -1 (red in the figure, Life Technologies). The negative control induced little dead cells, while the positive control Triton X induced widespread cell death. Note that gemcitabine is similar to the negative control with almost no induction of cell death, scale bar: 200 μm. **(b)** 10X microscope magnification was utilized for these images. Similarly, we noted that gemcitabine induces smaller PDOs (in white light images) vs. negative control, but no cell death, suggestive of cytostatic, but not cytocidal, effects, scale bar: 100 μm.

Supplementary Figure 3. **IC50 of Ponatinib in CCA8-7 and CCA8-11 lines.** The x-axis displays decreasing concentration of ponatinib, and the y-axis displays cell viability for each concentration of ponatinib. As shown, the IC50 for CCA8-7 is 4.2 μM and for CCA8-11 is 7.7 μM.

Supplementary Figure 4. Comparison of drug response data for PDO lines to the CCLE. The Cancer Cell Line Encyclopedia, CCLE, has drug response data for a number of cell-lines (26). For our purposes, we obtained the data for all of the available CCA and HCC cell-lines (n=20) that were tested using drugs in our screen (11 drugs). A list of the drug and cell-lines can be found in **Supplementary Table 1**. The highest dose used in the CCLE drug screen is 8 μM. Recall that our drug response data is for 10 μM. The results are shown in **(a)** a correlation matrix (generated using clustermap in Python with Pearson correlation metrics and the minimal variance method for hierarchical clustering, the colorbar represents the correlation), and **(b)** a plot of the first two principle components (showing the fraction of the variance in brackets, and the markers are colored based on clustering obtained using k-means algorithm with k=3). The clustering algorithm in **(a)** revealed two main clusters that predominantly corresponded to PDOs versus cell-lines. Interestingly, the drug response of the cell-line C3A clustered with the PDOs. Furthermore, there was a sub-group of cell-lines (the 10 cell lines from the bottom of the x-axis) that mostly had a poor correlation with the drug response from the PDOs.

Supplementary Figure 5. Comparison of drug response data for PDO lines to the GDSC. The Genomics of Drug Sensitivity in Cancer, GDSC, has drug response data for a number of cell-lines (27). Similar to **Supplementary Fig. 4**, we obtained the available data for CCA and HCC cell-lines (n=16). that were tested with drugs in our data set (29 unique drugs). Note that two of the drugs (olaparib and afatinib) have two different drug identification numbers with distinct drug response data in the GDSC and both were included in our analysis. The drugs in the GDSC are tested at different concentrations. We used the highest available drug dose (which in this data ranges from 0.5-16 μM). The results are shown in **(a)** a correlation matrix (generated using clustermap in Python with Pearson correlation metrics and the minimal variance method for hierarchical clustering, the colorbar represents the correlation), and **(b)** a plot of the first two principle components (showing the fraction of the variance in brackets, and the markers are

colored based on clustering obtained using k-means algorithm with k=3). The cell-line SK-HEP-1 was not included in **(b)** for illustrative purposes (since it was much higher on both the x and y-axes). Interestingly, there was a poor correlation between the drug response of this subset of data for the PDOs HCC26-2 and HCC26-3. Furthermore, the PDO HCC25-2 did not cluster with the remaining PDOs but instead with 6 of the cell-lines (brown cluster in **(b)**). These 6 cell-lines (found close to the top of the x-axis in **(a)**) mostly had a poor correlation with the drug response from the PDOs. Lastly, the cell-lines TGBC1TKB and SNU-449 clustered with the majority of the PDOs (light blue cluster in **(b)**).

Supplementary Figure 6. Construction of a phylogenetic tree based on genetic information. Phylogenetic tree, constructed using all somatic coding (missense, nonsense, and canonical splice site) single nucleotide variants (SNVs) exome-wide, based upon the maximum parsimony method with default parameters in MEGA7 (39). Branch length is proportional to the number of substitutions, with the reference line representing 500 exomic coding substitutions.

Supplementary Figure 7. Genetic, transcriptional and functional intra-tumor heterogeneity. **(a)** The 6 CCA PDO lines were grouped in an unsupervised analysis (principal components analysis). The difference among lines was the highest along principal component 1 (x-axis) and second highest along principal component 2 (y-axis). The raw data utilized to create this graph was the drug response levels to 129 drugs across the 6 PDO lines. Note that the 6 PDO lines cluster in 3 distinct groups based on their drug response resemblance. Similarly, a PCA analysis was performed using all somatic coding (missense, nonsense, and canonical splice site) single nucleotide variants (SNV's) exome-wide, across all six PDO lines from CCA8. Surprisingly, a different grouping is observed, although a total of 3 groups continues to be observed. Last, a PCA analysis was performed utilizing FPKM values generated from RNA sequencing data. The RNA PCA analysis shows the 6 PDO lines again self-organize in 3 groups which are distinct from the genetic grouping as well as functional grouping. **(b)** Graphic representation of inability of genetic

heterogeneity to predict either transcriptomic as well as functional heterogeneity. The genetic groupings are identified with a green, blue and red color, respectively. **(c)** Transcriptional heterogeneity cannot predict functional heterogeneity.

Supplementary Table 1. Cell Viability of a 129 drug library on CCA PDO line. CellTiter Glo was utilized for accurate and granular quantification of killing effect of a larger drug library on same CCA PDO line. A gradient color code was utilized to display the efficacy of drugs (red – efficacious, blue – ineffective), with drug names shown in **Supplementary Table 2**.

Supplementary Table 2. List of drug names displayed in Supplementary Table 1 and 13

Supplementary Table 3. Quantification of cell viability in clinical drug combinations for CCA. The numbers for cell viability demonstrated that drug combinations are as effective as the more effective of the 2 drugs that are part of the combination.

Supplementary Table 4. List of drug names displayed in Fig. 3a.

Supplementary Table 5. **Viability of 27 primary liver cancer PDOs after treatment with dasatinib.** The viability was measured with CellTiter Glo read 4 days after treatment with 10 μM dasatinib. Viability ranged from 0% to 100%. The data is color coded, with dark blue signifying 100% viability (no drug effect) and dark red signifying 0% viability (complete killing of cancer cells). Note that while dasatinib is moderately effective across CCA8, the intra-tumor drug response is highly variable. Moreover, there are other lines (such as PDO18, PDO22, and PDO24) where there was no measurable effect of dasatinib on cancer cells. The effectiveness spectrum of dasatinib is characteristic of the highly variable effects of tyrosine kinase inhibitors included in the 129 compound drug library that we tested across 27 PDO lines.

Supplementary Table 6. List of drug names displayed in Fig. 4a and 4b.

Supplementary Table 7. The most inter-patient divergent drugs are listed. To identify these drugs, we calculated the standard deviation of the 5 means (one per patient) for each drug, and ordered the data in decreasing order of the standard deviation (data not shown). We excluded

drugs that did not induce a significant cell killing in at least one of the 5 cancers (arbitrarily defined as at least 70% killing at a screening dose of 10 μM, based on our previous high-throughput drug screening experience). SD – standard deviation of cell viability after drug treatment.

Supplementary Table 8. Example of 14 drugs with low standard deviation of cell viability across 6 PDO lines isolated from patient CCA8. At the top of the table are drugs that are uniformly effective; at the bottom of the table are drugs that are uniformly ineffective.

Supplementary Table 9. The top intra-tumor divergent drugs for patient CCA8 are shown.

Supplementary Table 10. List of Drug names and cell lines for CCLE and GDSC data set for Supplementary Fig. 4 and 5.

Supplementary Table 11. Summary of CCA8 PDO exome sequencing results

Supplementary Table 12. 4 classes of drugs based on the drug effect on the PDOs

Supplementary Table 13. Ratio of cell viability readout in the 2 sister organoid lines. This table presents the ratio of cell viability in response to each of 129 cancer drugs as tested in 2 sister organoid lines. The 2 organoid lines were established from the same piece of cancer tissue. The names of the drugs are in **Supplementary Table 2.**

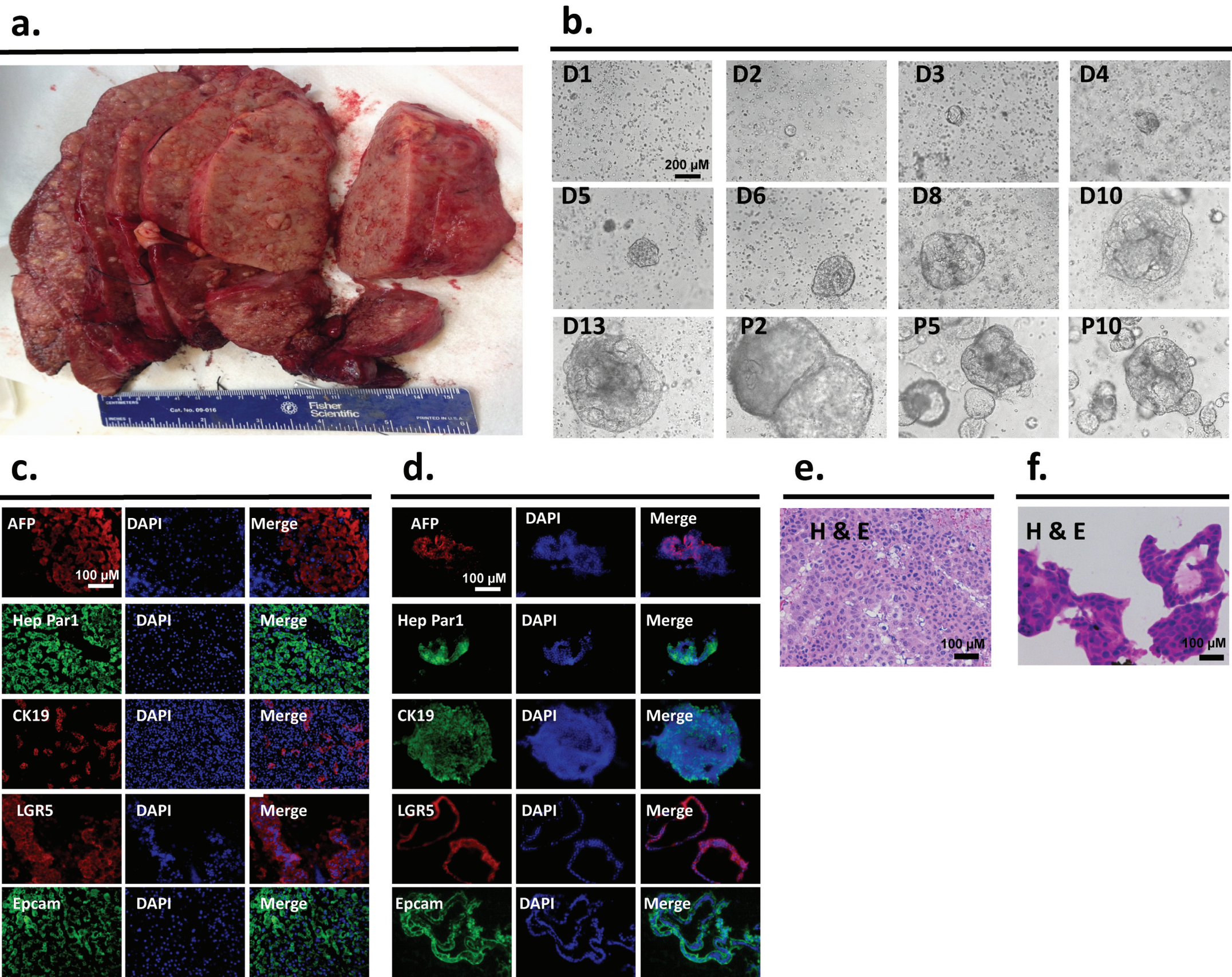
a.
b.
D1
200 μM
D2
D3
D4
D5
D6
D8
D10
D13
P2
P5
P10
c.
d.
e.
f.
AFP
DAPI
Merge
100 μM
Hep Par1
CK19
LGR5
Epcam
H & E

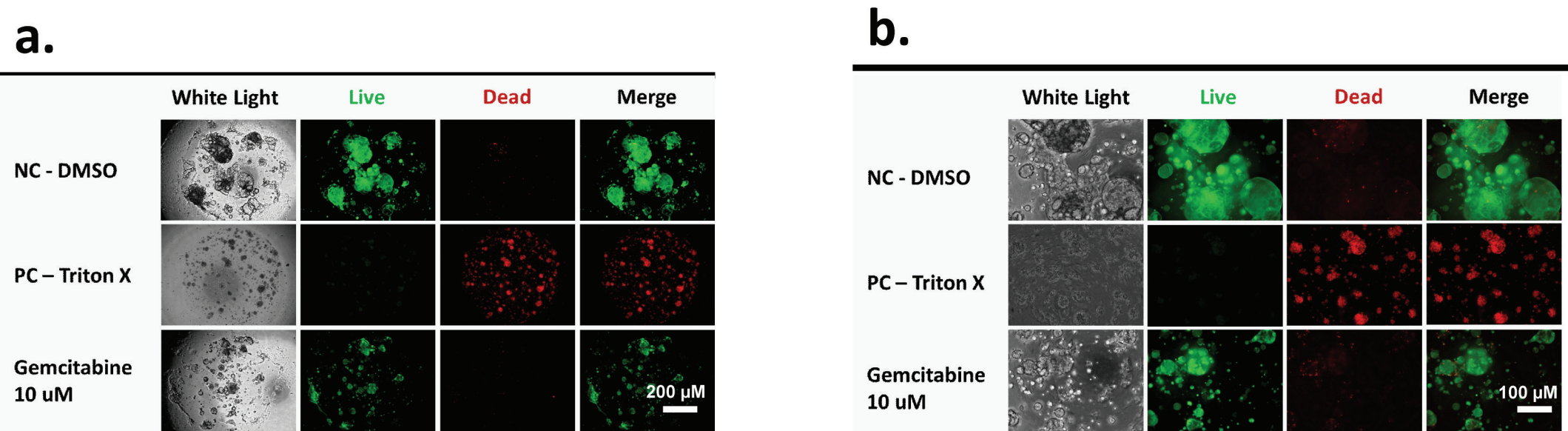
a.
White Light
Live
Dead
Merge
NC - DMSO
PC – Triton X
Gemcitabine
10 uM
200 µM
b.
White Light
Live
Dead
Merge
NC - DMSO
PC – Triton X
Gemcitabine
10 uM
100 µM

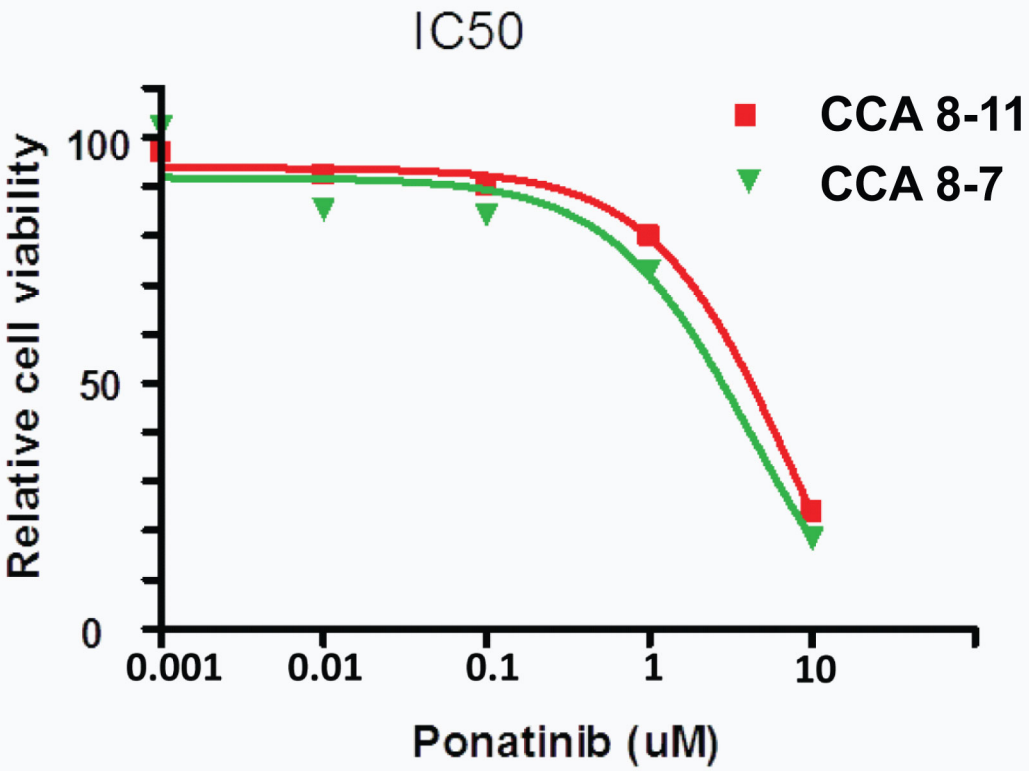

CCA 8-11 IC50: 7.787 uM

CCA 8-7 IC50: 4.22 uM

a.

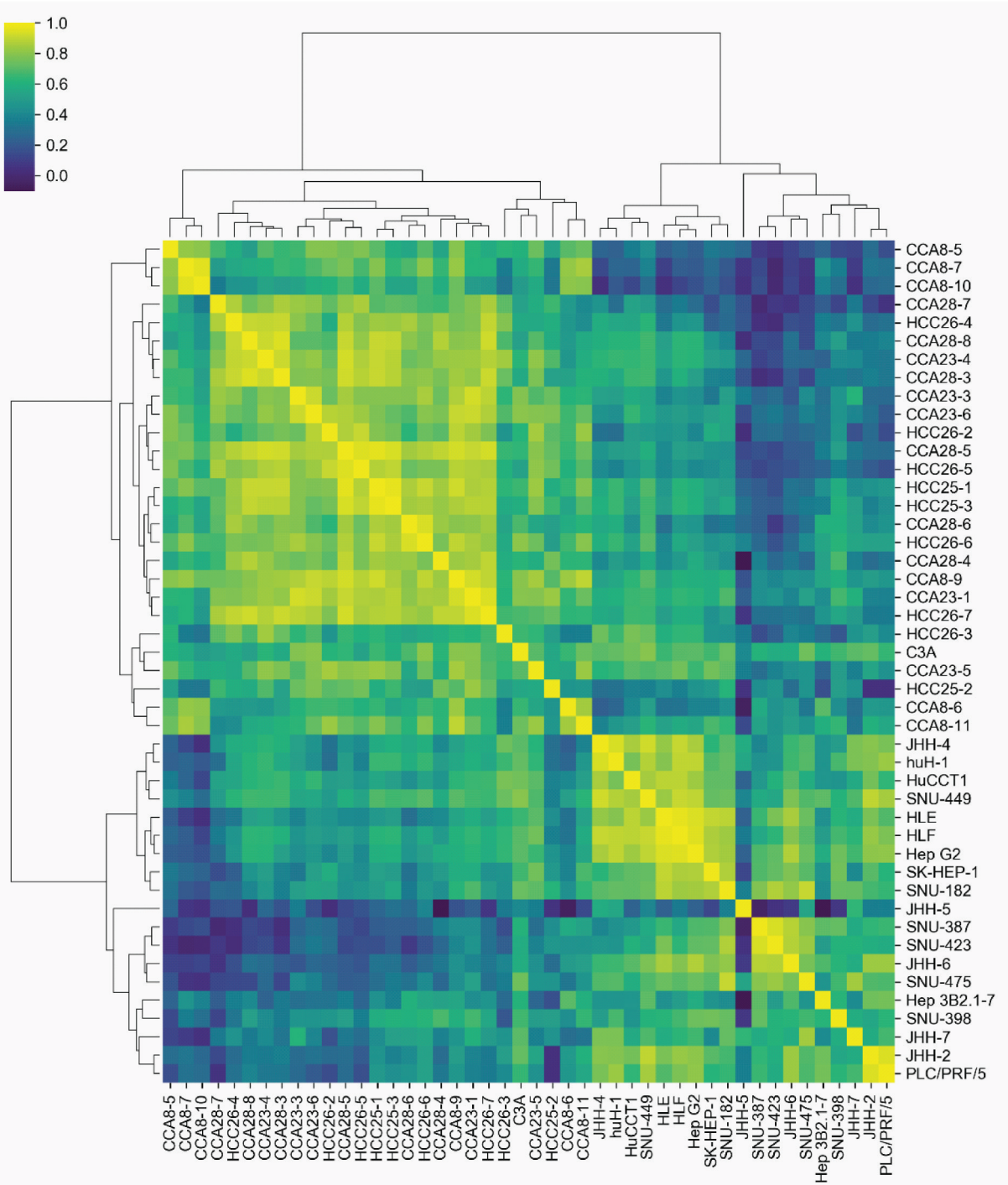
1.0
0.8
0.6
0.4
0.2
0.0
CCA8-5
CCA8-7
CCA8-10
CCA28-7
HCC26-4
CCA28-8
CCA23-4
CCA28-3
CCA23-3
CCA23-6
HCC26-2
CCA28-5
HCC26-5
HCC25-1
HCC25-3
CCA28-6
HCC26-6
CCA28-4
CCA8-9
CCA23-1
HCC26-7
HCC26-3
C3A
CCA23-5
HCC25-2
CCA8-6
CCA8-11
JHH-4
huH-1
HuCCT1
SNU-449
HLE
HLF
Hep G2
SK-HEP-1
SNU-182
JHH-5
SNU-387
SNU-423
JHH-6
SNU-475
Hep 3B2.1-7
SNU-398
JHH-7
JHH-2
PLC/PRF/5

b.

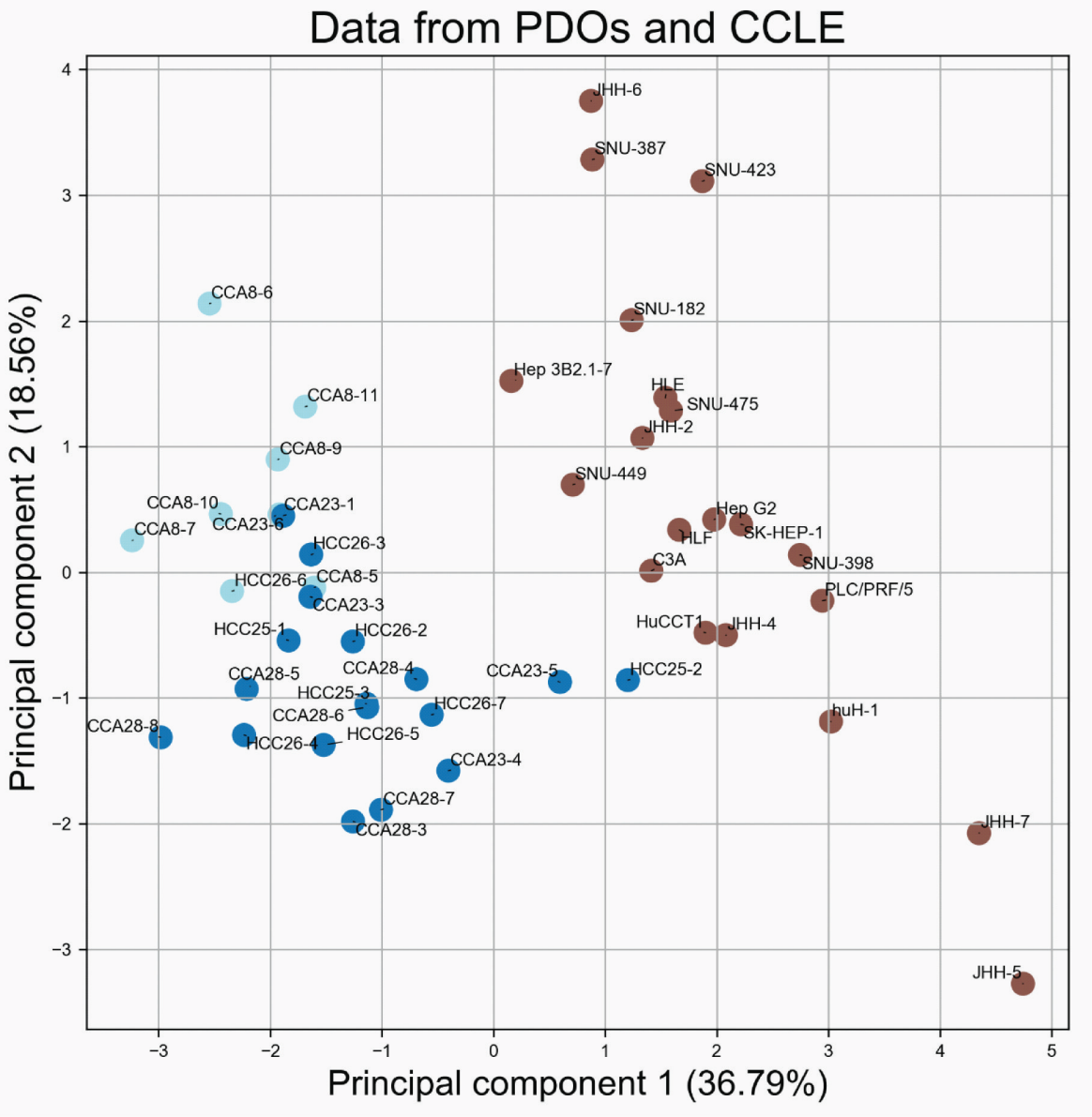
Data from PDOs and CCLE
Principal component 2 (18.56%)
Principal component 1 (36.79%)
JHH-6
SNU-387
SNU-423
CCA8-6
SNU-182
Hep 3B2.1-7
HLE
SNU-475
CCA8-11
JHH-2
CCA8-9
SNU-449
CCA8-10
CCA23-1
Hep G2
CCA8-7
CCA23-6
HLF
SK-HEP-1
HCC26-3
C3A
SNU-398
HCC26-6
CCA8-5
PLC/PRF/5
CCA23-3
HuCCT1
JHH-4
HCC25-1
HCC26-2
CCA28-5
CCA28-4
CCA23-5
HCC25-2
HCC25-3
HCC26-7
CCA28-6
huH-1
CCA28-8
HCC26-4
HCC26-5
CCA23-4
CCA28-7
CCA28-3
JHH-7
JHH-5

a.

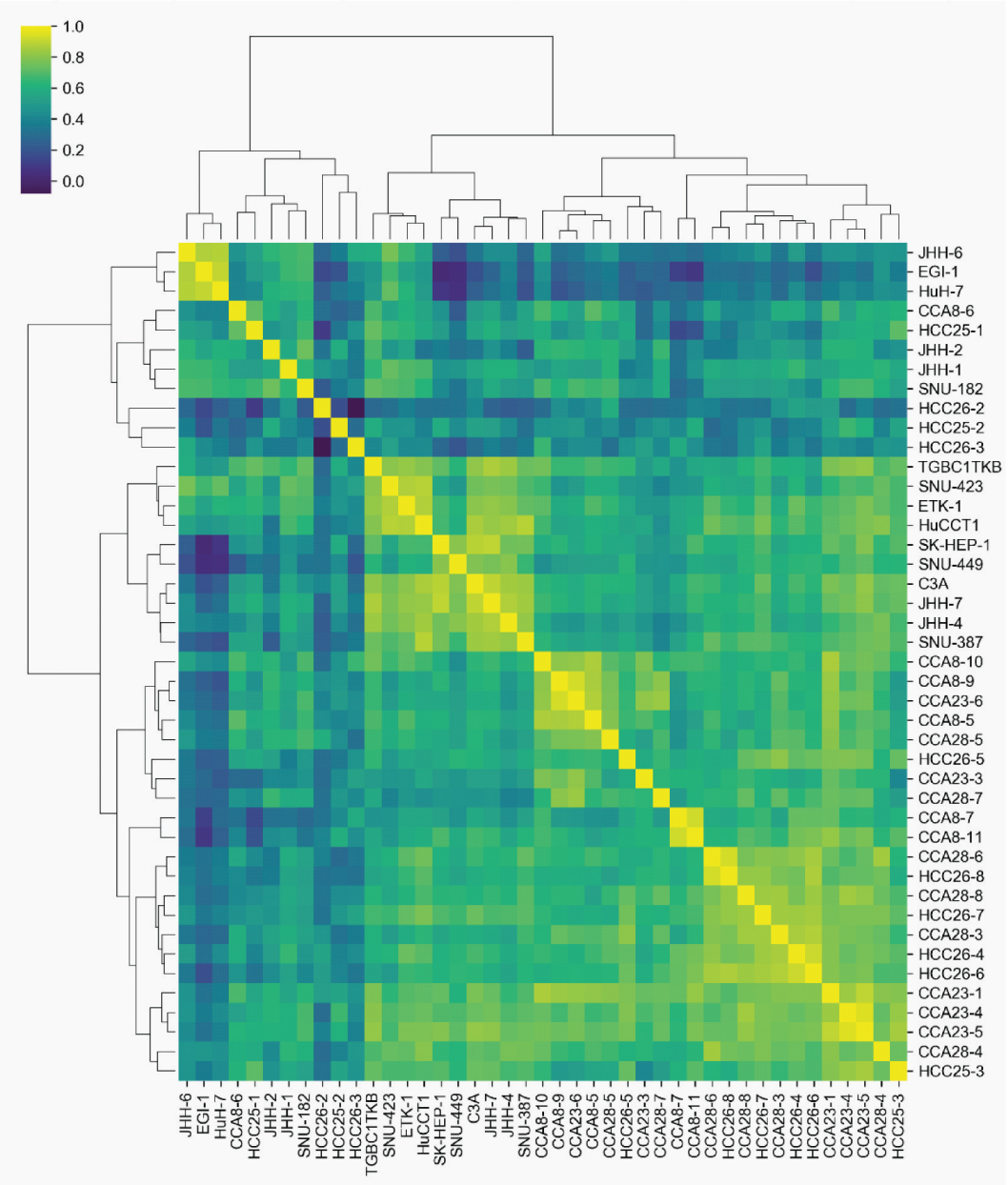
1.0
0.8
0.6
0.4
0.2
0.0
JHH-6
EGI-1
HuH-7
CCA8-6
HCC25-1
JHH-2
JHH-1
SNU-182
HCC26-2
HCC25-2
HCC26-3
TGBC1TKB
SNU-423
ETK-1
HuCCT1
SK-HEP-1
SNU-449
C3A
JHH-7
JHH-4
SNU-387
CCA8-10
CCA8-9
CCA23-6
CCA8-5
CCA28-5
HCC26-5
CCA23-3
CCA28-7
CCA8-7
CCA8-11
CCA28-6
HCC26-8
CCA28-8
HCC26-7
CCA28-3
HCC26-4
HCC26-6
CCA23-1
CCA23-4
CCA23-5
CCA28-4
HCC25-3

b.

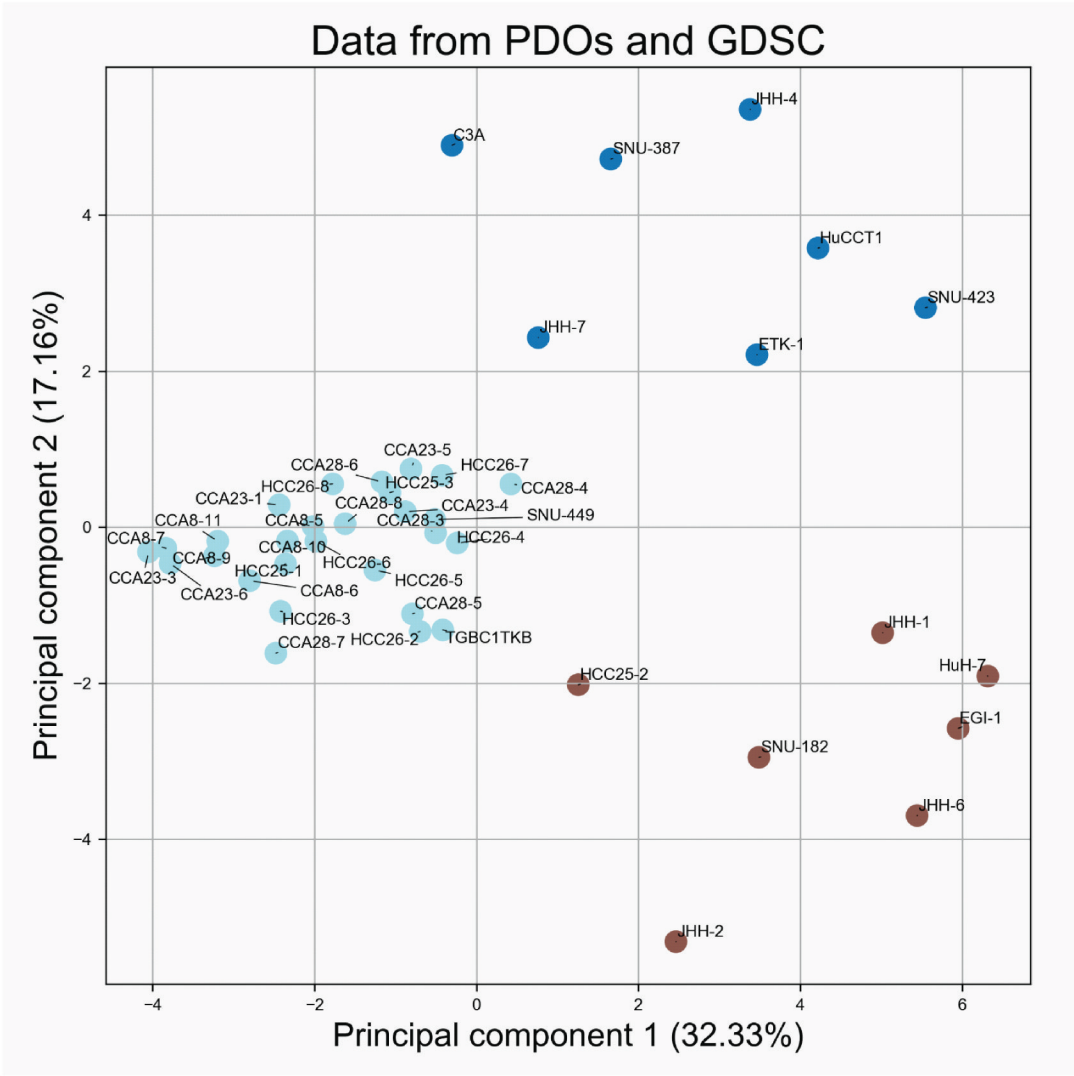
Data from PDOs and GDSC
Principal component 2 (17.16%)
Principal component 1 (32.33%)
JHH-4
C3A
SNU-387
HuCCT1
SNU-423
JHH-7
ETK-1
CCA23-5
CCA28-6
HCC26-7
HCC26-8
HCC25-3
CCA28-4
CCA23-1
CCA28-8
CCA23-4
SNU-449
CCA8-11
CCA8-5
CCA28-3
HCC26-4
CCA8-7
CCA8-10
CCA8-9
HCC26-6
HCC25-1
HCC26-5
CCA23-3
CCA8-6
CCA23-6
CCA28-5
HCC26-3
JHH-1
CCA28-7
HCC26-2
TGBC1TKB
HuH-7
HCC25-2
EGI-1
SNU-182
JHH-6
JHH-2

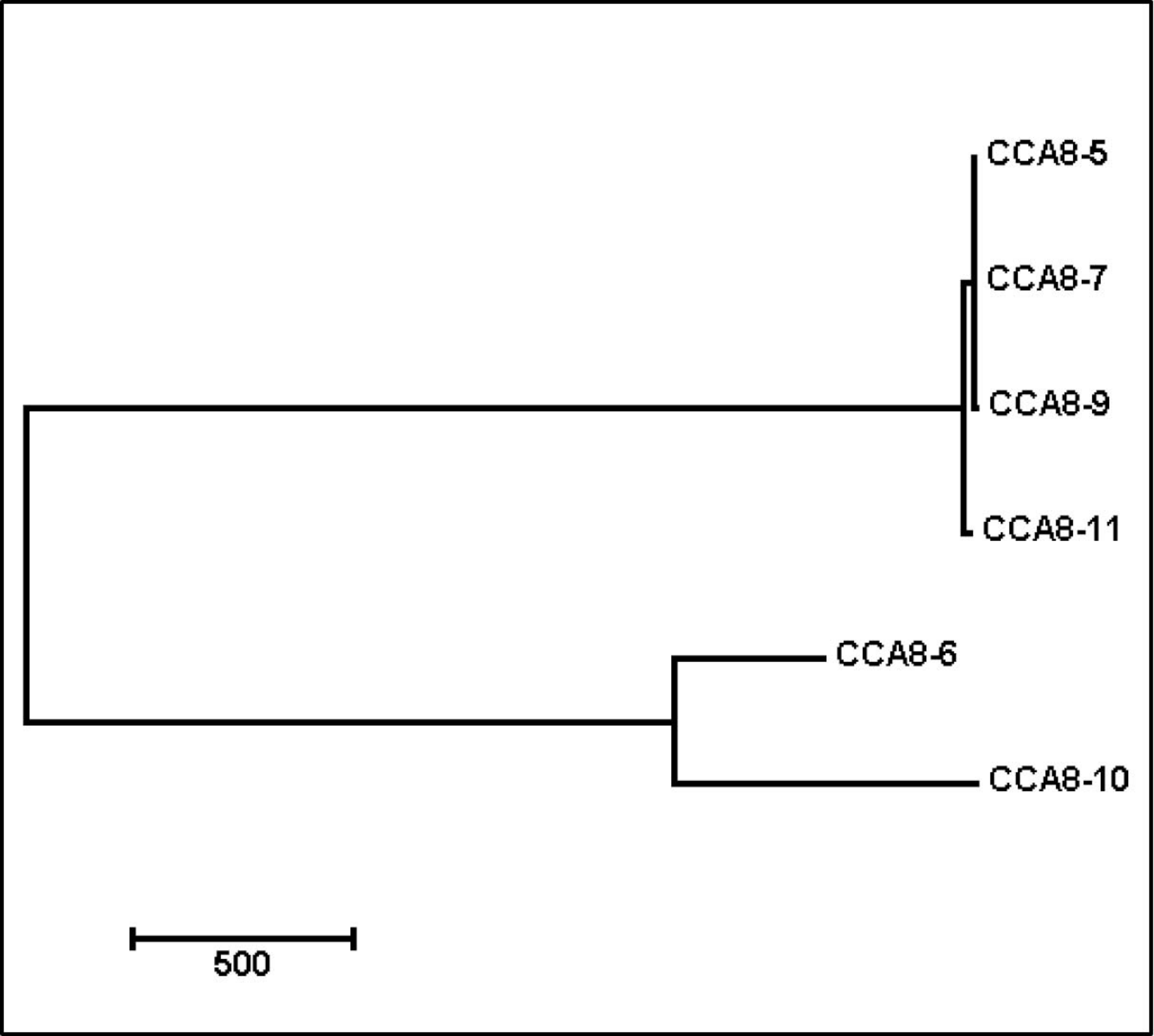
CCA8-5
CCA8-7
CCA8-9
CCA8-11
CCA8-6
CCA8-10
500

a.

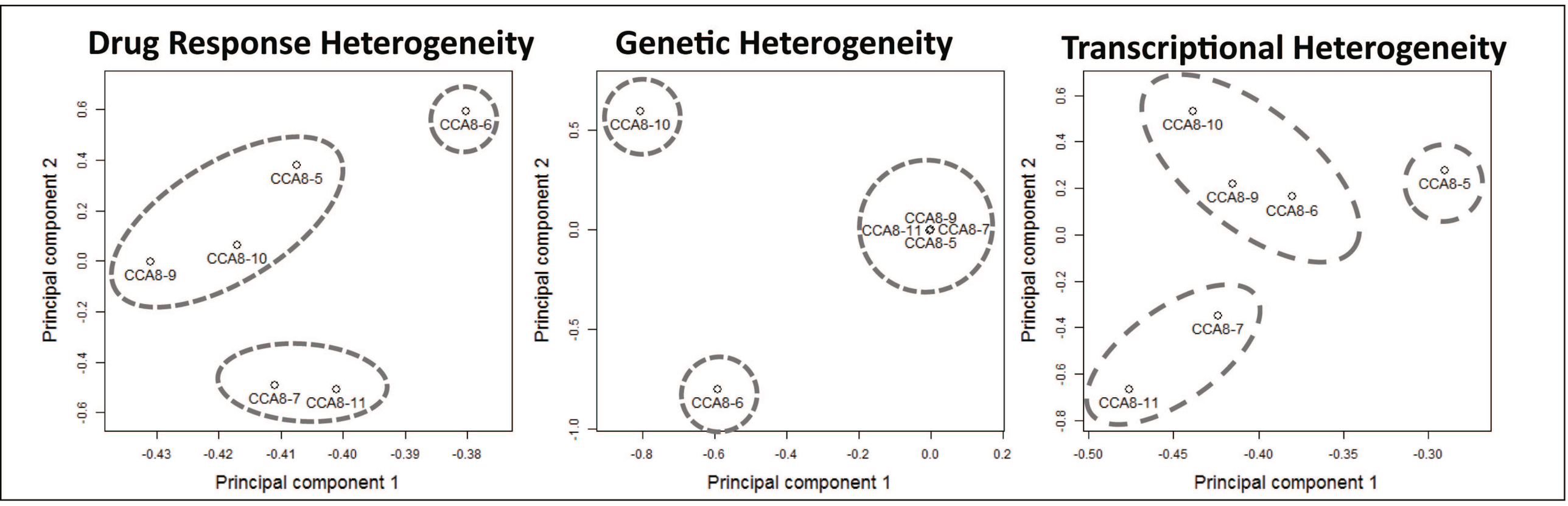
Drug Response Heterogeneity
Genetic Heterogeneity
Transcriptional Heterogeneity
Principal component 1
Principal component 2
CCA8-6
CCA8-5
CCA8-10
CCA8-9
CCA8-7
CCA8-11

b.

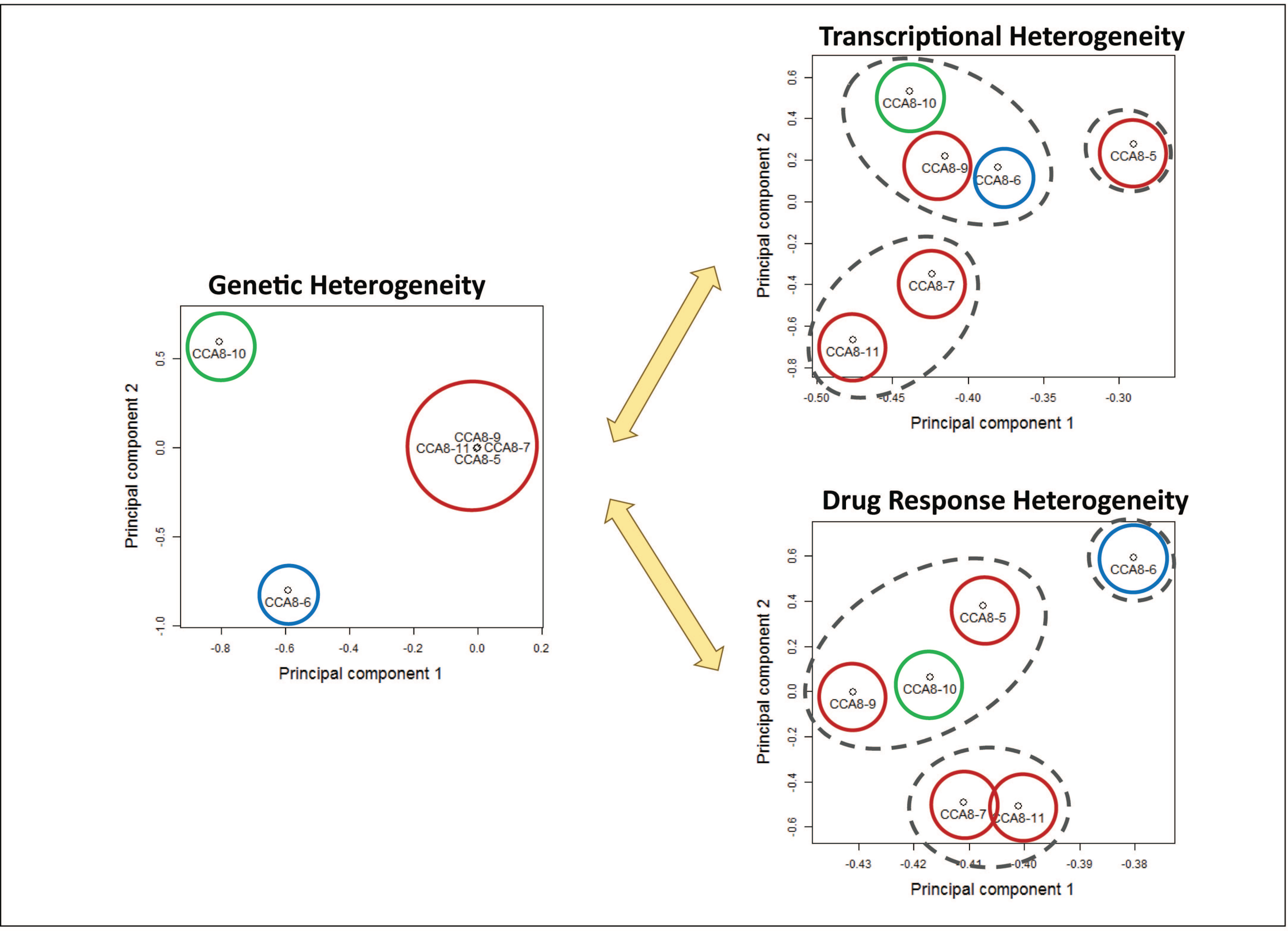
Transcriptional Heterogeneity
Genetic Heterogeneity
Drug Response Heterogeneity
Principal component 1
Principal component 2
CCA8-10
CCA8-9
CCA8-6
CCA8-5
CCA8-7
CCA8-11

c.

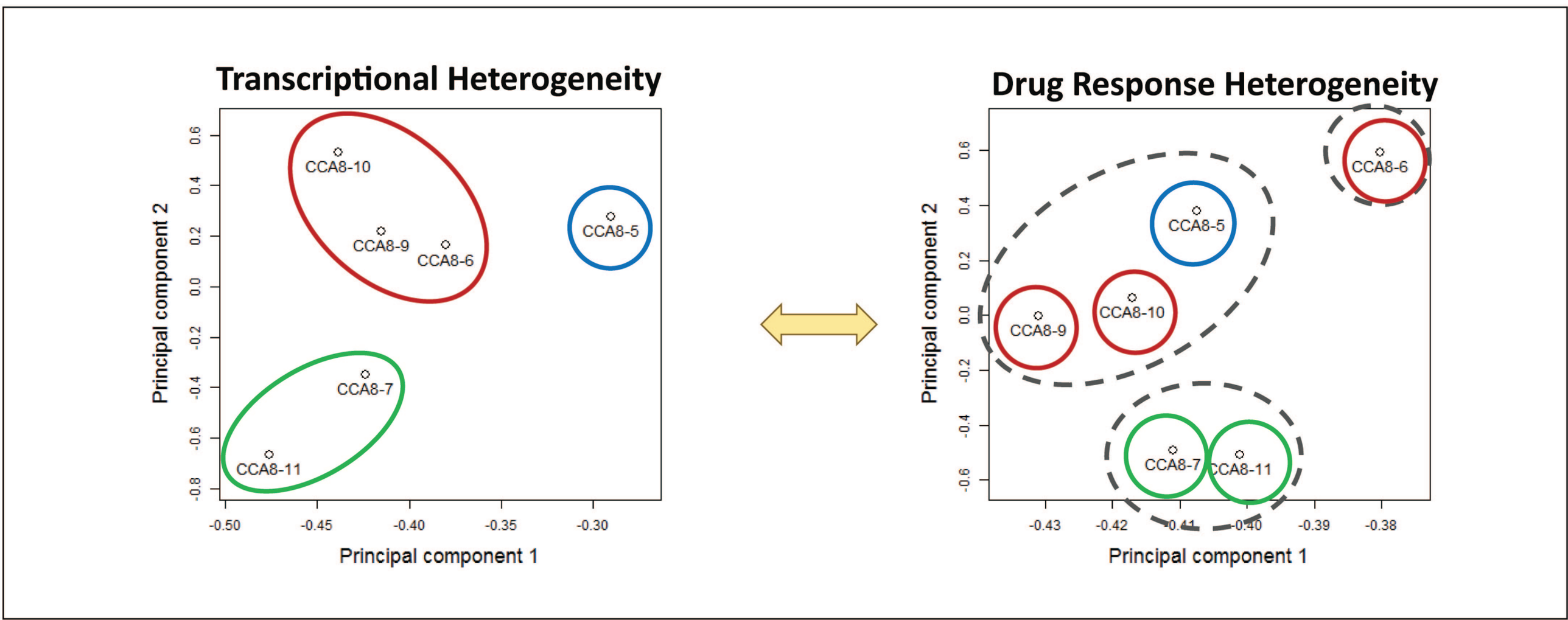
Transcriptional Heterogeneity
Drug Response Heterogeneity
Principal component 1
Principal component 2
CCA8-10
CCA8-9
CCA8-6
CCA8-5
CCA8-7
CCA8-11